IAEA nuclear fusion

PAPER • **OPEN ACCESS**

Nonlinear saturation of toroidal Alfvén eigenmodes via ion induced scattering in nonuniform plasmas

To cite this article: Zhiwen Cheng *et al* 2025 *Nucl. Fusion* **65** 082002

OPEN ACCESS
IOP Publishing | International Atomic Energy Agency

Nuclear Fusion

Nucl. Fusion **65** (2025) 082002 (8pp)

https://doi.org/10.1088/1741-4326/adeff0

Nonlinear saturation of toroidal Alfvén eigenmodes via ion induced scattering in nonuniform plasmas

Zhiwen Cheng[1], Kexun Shen[1], Liu Chen[1,2], Fulvio Zonca[2,1] and Zhiyong Qiu[3,*]

[1] Institute for Fusion Theory and Simulation, School of Physics, Zhejiang University, Hangzhou 310027, China
[2] Center for Nonlinear Plasma Science, ENEA C.R. Frascati, Frascati 00044, Italy
[3] CAS Key Laboratory of Frontier Physics in Controlled Nuclear Fusion and Institutes of Plasma Physics, Chinese Academy of Sciences, Hefei 230031, China

E-mail: zqiu@ipp.ac.cn

Received 6 April 2025, revised 14 June 2025
Accepted for publication 15 July 2025
Published 24 July 2025

CrossMark

Abstract

In nonuniform plasmas, toroidal Alfvén eigenmode (TAE) is shown to decay into high toroidal mode number modes due to ion induced scattering (Cheng *et al* 2024 *Nucl. Fusion* **64** 066031). In this work, the three wave parametric decay model is generalized into reactor-relevant multiple-mode case, and the wave-kinetic equation describing the TAE spectrum evolution in k_θ space due to ion induced scattering is derived. Here, k_θ is the poloidal wavenumber. By numerically solving the wave-kinetic equation with reactor-relevant parameters, the nonlinear evolution and saturation process of TAE spectral intensity is derived, which yields a saturation spectrum consistent with the fixed point solution. It is found that the magnetic perturbation amplitude induced by the TAE saturation spectrum is lower than the uniform plasma result due to the enhanced nonlinear coupling by plasma nonuniformity. Potential impact on intrinsic plasma rotation is also discussed.

Keywords: toroidal Alfvén eigenmode, ion induced scattering, nonlinear saturation, gyrokinetic theory

(Some figures may appear in colour only in the online journal)

1. Introduction

In next-generation fusion reactors like ITER [1], the power density of energetic particles (EPs), in particular fusion alpha particles, is comparable to that of the bulk thermal plasma. With the EP characteristic frequencies being comparable with Alfvén frequency and EP characteristic orbit size being much smaller than the device size, a variety of shear Alfvén wave (SAW) instabilities [2] could be resonantly excited [3–6], and consequently, induce considerable EP anomalous transport [7–10]. Transport loss of EPs across the magnetic surfaces could then result in significantly reduced plasma heating efficiency, disastrous degradation of plasma performance, and even severe damage to plasma facing components by the associated heat flux [11, 12]. The EP anomalous transport rate is mainly determined by the electromagnetic perturbations induced by SAW instabilities, it is, thus, crucial to investigate their nonlinear evolution and saturation process [7, 13, 14].

* Author to whom any correspondence should be addressed.

In toroidally confined devices, the periodic modulation of Alfvén speed v_{A} along the equilibrium magnetic field renders the formation of frequency gaps inside the SAW continuum. SAW instabilities generally exhibit themselves as EP modes [15] or discrete Alfvén eigenmodes (AEs) [16–21] inside the continuum gaps, among which the toroidal Alfvén eigenmode (TAE) is considered as one of the most important candidates responsible for EP anomalous transport. Taking TAE as a representative paradigm, nonlinear mode coupling mechanisms contributing to its saturation have been widely investigated [4, 22–25], including nonlinear excitation of high frequency harmonics by TAE mode coupling [26, 27], nonlinear generation of zonal structure via modulational instability or self-beating processes [23, 28, 29], and nonlinear scattering by drift wave [30, 31].

Another crucial mode coupling channel is the ion induced scattering of TAE, in which a pump TAE decays into a counter-propagating sideband TAE and an ion sound wave quasi-mode. This mechanism was originally investigated in [22] in long wavelength regime with $k_\perp^2\rho_{\mathrm{i}}^2 \ll \omega/\Omega_{\mathrm{ci}}$ and dominant ion density nonlinearity. Here, ρ_{i} and Ω_{ci} are the ion Larmor radius and cyclotron frequency, respectively. Based on drift kinetic theory, the wave-kinetic equation describing the TAE spectral energy transfer and the corresponding magnetic perturbation induced by TAE is derived [22]. Later, it was extended to the short wavelength regime with $k_\perp^2\rho_{\mathrm{i}}^2 \gg \omega/\Omega_{\mathrm{ci}}$ using nonlinear gyrokinetic theory, where perpendicular nonlinearity dominates [32]. The corresponding wave-kinetic equation was derived and the TAE induced magnetic perturbation amplitude was estimated, which showed a significant reduction compared to the long wavelength limit result, due to the enhanced perpendicular coupling [33]. Correspondingly, the resultant EP transport rate was also derived, showing a strong dependence on the inverse aspect ratio of the torus.

While the previous works on parametric decay process generally assumed uniform plasmas, it is found in recent research that plasma nonuniformity can both quantitatively and qualitatively modify the parametric decay process of kinetic Alfvén waves (KAWs) [34]. Here, plasma nonuniformity refers particularly to the profile of plasma density or temperature, contributing to the ion diamagnetic drift frequency $\omega_{*\mathrm{i}}^{\mathrm{t}}$. Considering the process of a pump KAW decaying into a counter-propagating KAW and a drift sound wave (DSW) in nonuniform plasmas with $\omega_{*\mathrm{i}}^{\mathrm{t}}$ being much larger than ion transit frequency, it is found that quantitatively the nonlinear coupling coefficient is enhanced by an order of magnitude, while qualitatively, the parity breaking of the KAW spectrum results in considerable convective plasma transport and possible confinement improvement.

Motivated by [34], effects of plasma nonuniformity on the parametric decay process of TAE was investigated in [35], where the process of a pump TAE decaying into sideband TAE and DSW quasi-mode was considered. The corresponding parametric dispersion relation was derived and analysed. It is found that, the nonlinear scattering cross-section of this parametric decay process is significantly enhanced as expected, and the spontaneous decay condition is modified qualitatively. To be more specific, in uniform plasmas, pump TAE spontaneously decays into sideband TAE with lower frequency, while in nonuniform plasmas, it decays into sideband TAE with higher toroidal mode number n. Considering burning plasmas in ITER-like tokamaks where a rich spectrum of TAEs exist, the nonlinear evolution behaviour of TAE spectrum could be significantly influenced due to this ion induced scattering process. Moreover, effects of plasma nonuniformity are anticipated to render an evolution towards larger toroidal mode number, which could bring considerable momentum transport and related plasma rotation, contributing potentially to the improvement of plasma confinement [36–38].

In the present work, we extend the three wave parametric dispersion relation into multiple-mode case to investigate the nonlinear evolution of TAE spectrum in nonuniform plasmas. Specifically, based on the parametric dispersion relation obtained previously, the wave-kinetic equation describing the nonlinear evolution of test TAE due to interaction with multiple background TAEs is derived. Given that TAE decays in k_θ in nonuniform plasmas, we adopt the continuum approximation and perform the mode summation by integrating in k_θ space. The wave-kinetic equation describing the nonlinear evolution and saturation process of the TAE spectrum is then derived and analysed. Numerically, solving it as an initial value problem, the evolution of TAE spectrum to the steady state can be obtained. On the other hand, transforming the wave-kinetic equation into a fixed point form, numerical solution of the TAE saturation spectrum can be obtained directly. Analytically, this fixed point form equation can also be solved, and the saturation spectrum in both long wavelength and short wavelength limits can be derived. For better comprehension, with reactor-relevant parameters, the TAE saturation spectrums by both initial value solution and fixed point solution are provided, which show great agreement with each other. The overall magnetic perturbation amplitude induced by TAE spectrum is also provided.

The rest of this paper is organised as follows. In section 2, the derivation of parametric dispersion relation is briefly reviewed. In section 3, the wave-kinetic equation and the corresponding fixed point form are derived. In section 4, based on the fixed point form equation, the saturation spectrum is solved analytically in both long and short wavelength limits, and a comparison with numerical solution is provided. Section 5 shows the nonlinear evolution and saturation process of TAE spectrum under reactor-relevant parameters, with the corresponding saturation amplitude provided. In section 6, conclusion and discussion are given.

2. Review of the parametric dispersion relation

In this section, the derivation of parametric dispersion relation describing TAE ion induced scattering, originally presented in [35], is briefly reviewed, as a starting point of subsequent analyses on TAE spectrum evolution.

In this parametric decay model, a test TAE $\Omega_0 = (\omega_0, \boldsymbol{k}_0)$ is considered to couple with a counter-propagating background

TAE $\Omega_1=(\omega_1,\boldsymbol{k}_1)$, and generate a DSW quasi-mode $\Omega_s=(\omega_s,\boldsymbol{k}_s)$. For the considered low-β plasma with β being the ratio between thermal and magnetic pressures, the field perturbations can be represented by the scalar potential $\delta\phi$ and parallel vector potential $\delta A_\parallel$, and an alternative field variable $\delta\psi\equiv\omega\delta A_\parallel/(ck_\parallel)$ is introduced for convenience, with $\delta\phi=\delta\psi$ corresponding to ideal MHD condition. Without loss of generality, taking the matching condition as $\Omega_0=\Omega_1+\Omega_s$ and following the standard procedure of gyrokinetic theory [39], the governing equations can be derived from the quasi-neutrality condition and nonlinear gyrokinetic vorticity equation shown as below.

Specifically, for electrostatic modes like DSW, the mode equation can be derived from the quasi-neutrality condition,

$$\frac{N_0e^2}{T_\mathrm{i}}\left(1+\frac{T_\mathrm{i}}{T_\mathrm{e}}\right)\delta\phi_k=\sum_{\mathrm{j=e,i}}\langle qJ_k\delta H_k\rangle_\mathrm{j}. \tag{1}$$

Here, N_0 is the equilibrium particle density, T_j and q_j are respectively the temperature and charge, with $\mathrm{j=e,i}$ standing for electron or ion. $J_k\equiv J_0(k_\perp\rho)$ accounts for finite Larmor radius (FLR) effects with J_0 being the Bessel function of the first kind, and δH_k is the non-adiabatic particle response derived from the following nonlinear gyrokinetic equation [39]

$$\begin{aligned}\left(-\mathrm{i}\omega+v_\parallel\partial_l+\mathrm{i}\omega_\mathrm{d}\right)\delta H_k=&\,\mathrm{i}\frac{q}{m}\left(\omega\partial_E+\frac{m}{T}\omega_*\right)F_\mathrm{M}J_k\delta L_k\\&-\sum_{\boldsymbol{k}=\boldsymbol{k}'+\boldsymbol{k}''}\Lambda^{k'}_{k''}J_{k'}\delta L_{k'}\delta H_{k''},\end{aligned} \tag{2}$$

with ∂_l representing the derivative along the field line, $\omega_\mathrm{d}=(v_\perp^2+2v_\parallel^2)/(2\Omega_cR)(k_r\sin\theta+k_\theta\cos\theta)$ standing for the magnetic drift frequency, R being the major radius and $\omega_{*\mathrm{j}}=-\mathrm{i}(cT/qB_0)_\mathrm{j}\hat{\boldsymbol{b}}\times\nabla\ln N_\mathrm{j}\cdot\nabla$ being the diamagnetic drift frequency induced by plasma density nonuniformity, while plasma temperature nonuniformity is neglected to simplify the analysis. Furthermore, F_M is the Maxwellian distribution function, $\delta L_k\equiv\delta\phi_k-k_\parallel v_\parallel\delta\psi_k/\omega_k$ is the scalar potential in the guiding-centre frame and $\Lambda^{k'}_{k''}=(c/B_0)\hat{\boldsymbol{b}}\cdot\boldsymbol{k}''\times\boldsymbol{k}'$ stands for the perpendicular nonlinear coupling with the constraint of matching condition.

Substituting the non-adiabatic particle responses to DSW into the quasi-neutrality equation, one obtains the equation of DSW generation due to TAEs nonlinear coupling

$$\varepsilon_{\mathrm{s}*}\delta\phi_\mathrm{s}=-\mathrm{i}\frac{\Lambda^1_0}{\omega_0}\alpha_{\mathrm{s}*}\delta\phi_0\delta\phi_{1*}. \tag{3}$$

Here, $\varepsilon_{\mathrm{s}*}\equiv1+\tau+\tau\Gamma_\mathrm{s}\xi_\mathrm{s}Z(\xi_\mathrm{s})(1-\omega_{*\mathrm{i,s}}/\omega_\mathrm{s})$ is the linear dispersion relation of Ω_s, $\alpha_{\mathrm{s}*}\equiv\tau F_1[1+\xi_\mathrm{s}Z(\xi_\mathrm{s})(1-\omega_{*\mathrm{i,s}}/\omega_\mathrm{s})]+\sigma_{0*}\sigma_{1*}$ is the nonlinear coupling coefficient, $\tau\equiv T_\mathrm{e}/T_\mathrm{i}$, $\Gamma_k\equiv\langle J_k^2F_\mathrm{M}/N_0\rangle$, $F_1\equiv\langle J_0J_1J_\mathrm{s}F_\mathrm{M}/N_0\rangle$ with $\langle\cdots\rangle$ accounting for velocity space integration, $Z(\xi_\mathrm{s})$ is the well-known plasma dispersion function with $\xi_\mathrm{s}\equiv\omega/|k_{\parallel\mathrm{s}}v_\mathrm{i}|$, and $\sigma_{k*}\equiv[1+\tau-\tau\Gamma_k(1-\omega_{*\mathrm{i},k}/\omega_k)]/(1-\omega_{*\mathrm{e},k}/\omega_k)$ is the ratio between $\delta\psi$ and $\delta\phi$. In deriving equation (3), the expressions $\delta H^\mathrm{L}_\mathrm{s,e}=0$, $\delta H^\mathrm{L}_\mathrm{s,i}=(e/T_\mathrm{i})(\omega_\mathrm{s}-\omega_{*\mathrm{i,s}})/(\omega_\mathrm{s}-k_{\parallel\mathrm{s}}v_\parallel)F_\mathrm{M}J_\mathrm{s}\delta\phi_\mathrm{s}$, $\delta H^\mathrm{L}_\mathrm{T,e}=-(e/T_\mathrm{e})[1-(\omega_{*\mathrm{e,T}}/\omega_\mathrm{T})]F_\mathrm{M}\delta\psi_\mathrm{T}$, $\delta H^\mathrm{L}_\mathrm{T,i}=(e/T_\mathrm{i})[1-(\omega_{*\mathrm{i,T}}/\omega_\mathrm{T})]F_\mathrm{M}J_\mathrm{T}\delta\phi_\mathrm{T}$, $\delta H^\mathrm{NL}_\mathrm{s,e}=\mathrm{i}(\Lambda^1_0/\omega_0)(e/T_\mathrm{e})F_\mathrm{M}\delta\psi_0\delta\psi_{1*}$ and $\delta H^\mathrm{NL}_\mathrm{s,i}=\mathrm{i}(\Lambda^1_0/\omega_0)(e/T_\mathrm{i})F_\mathrm{M}J_0J_1(k_{\parallel\mathrm{s}}v_\parallel-\omega_{*\mathrm{i,s}})/(\omega_\mathrm{s}-k_{\parallel\mathrm{s}}v_\parallel)\delta\phi_0\delta\phi_{1*}$ are used, with the subscript $\mathrm{T}=0,1$ representing test and background TAEs. Interested readers may refer to [35] for the detailed derivation.

For electromagnetic mode like TAE, the nonlinear gyrokinetic vorticity equation is also required to close the system,

$$\begin{aligned}&\frac{c^2}{4\pi\omega_k^2}B\frac{\partial}{\partial l}\frac{k_\perp^2}{B}\frac{\partial}{\partial l}\delta\psi_k+\frac{N_0e^2}{T_\mathrm{i}}\left(1-\frac{\omega_{*\mathrm{i}}}{\omega}\right)_k(1-\Gamma_k)\delta\phi_k\\&\quad-\sum_{\mathrm{j=e,i}}\left\langle qJ_0\frac{\omega_\mathrm{d}}{\omega}\delta H\right\rangle_k\\&=-\frac{\mathrm{i}}{\omega_k}\sum_{\boldsymbol{k}=\boldsymbol{k}'+\boldsymbol{k}''}\Lambda^{k'}_{k''}\left[\langle e\,(J_kJ_{k'}-J_{k''})\,\delta L_{k'}\delta H_{k''}\rangle\right.\\&\quad\left.+\frac{c^2}{4\pi}k_\perp''^2\frac{\partial_l\delta\psi_{k'}\partial_l\delta\psi_{k''}}{\omega_{k'}\omega_{k''}}\right].\end{aligned} \tag{4}$$

Here, the terms on the left hand side stand for the field line bending, inertia and curvature pressure coupling respectively, while terms on the right hand side represent the gyrokinetic Reynolds stress and Maxwell stress, which are the dominant perpendicular nonlinear terms in the short wavelength regime. In the present case, due to the electrostatic property of sideband DSW, here the Maxwell stress is generally negligible.

Substituting the corresponding particle responses into equations (1) and (4), we obtain the nonlinear equation of the test TAE,

$$\left[\varepsilon_{\mathrm{A}0}+\left(\frac{\Lambda^1_0}{\omega_0}\right)^2\varepsilon^\mathrm{NL}_{\mathrm{A}0}|\delta\phi_1|^2\right]\delta\phi_0=\mathrm{i}\frac{\Lambda^1_0}{\omega_0}\alpha_{0*}\delta\phi_1\delta\phi_\mathrm{s}. \tag{5}$$

Here, $\varepsilon_{\mathrm{A}0}\equiv(1-\Gamma_0)(1-\omega_{*\mathrm{i},0}/\omega_0)/b_0-k^2_{\parallel0}v^2_\mathrm{A}\sigma_{0*}/\omega_0^2$ is the linear dispersion relation of the test TAE, $\varepsilon^\mathrm{NL}_{\mathrm{A}0}\equiv[(F_2-F_1)/b_0-k^2_{\parallel0}v^2_\mathrm{A}\tau F_2/\omega_0^2][1+\xi_\mathrm{s}Z(\xi_\mathrm{s})(1-\omega_{*\mathrm{i,s}}/\omega_\mathrm{s})]+k^2_{\parallel0}v^2_\mathrm{A}\sigma_{0*}\sigma^2_{1*}/\omega_0^2$, and $\alpha_{0*}\equiv(1/b_0-\tau k^2_{\parallel0}v^2_\mathrm{A}/\omega_0^2)[1+\xi_\mathrm{s}Z(\xi_\mathrm{s})(1-\omega_{*\mathrm{i,s}}/\omega_\mathrm{s})]F_1+(\sigma_{1*}-\varepsilon_{\mathrm{s}*})/(\tau b_0)$ are the nonlinear coupling coefficients between test TAE and DSW, with $b_0\equiv k_\perp^2\rho_\mathrm{i}^2/2$ and $F_2\equiv\langle J_0^2J_1^2F_\mathrm{M}/N_0\rangle$. In deriving this equation, the expressions for test TAE nonlinear responses $\delta H^\mathrm{NL}_\mathrm{0,e}=\left(\Lambda^1_0/\omega_0\right)^2(e/T_\mathrm{e})F_\mathrm{M}|\delta\psi_1|^2\delta\psi_0$ and $\delta H^\mathrm{NL}_\mathrm{0,i}=-\mathrm{i}(\Lambda^1_0/\omega_0)(e/T_\mathrm{i})F_\mathrm{M}J_1J_\mathrm{s}(k_{\parallel\mathrm{s}}v_\parallel-\omega_{*\mathrm{i,s}})/(\omega_\mathrm{s}-k_{\parallel\mathrm{s}}v_\parallel)\delta\phi_1\delta\phi_\mathrm{s}-\left(\Lambda^1_0/\omega_0\right)^2(e/T_\mathrm{i})F_\mathrm{M}J_0J_1^2(k_{\parallel\mathrm{s}}v_\parallel-\omega_{*\mathrm{i,s}})/(\omega_\mathrm{s}-k_{\parallel\mathrm{s}}v_\parallel)|\delta\phi_1|^2\delta\phi_0$ are also used.

The parametric dispersion relation can be derived from equations (3) and (5),

$$\varepsilon_{\mathrm{A}0}|\delta\phi_0|^2=-\left(\Delta+\chi_0\varepsilon_{\mathrm{s}*}-\frac{C_0}{\varepsilon_{\mathrm{s}*}}\right)|\delta\phi_0|^2|\delta\phi_1|^2. \tag{6}$$

Here, $\Delta\equiv(\Lambda^1_0/\omega_0)^2[\sigma^2_{0*}\sigma_{1*}-2(F_1/\Gamma_\mathrm{s})(\sigma_{0*}\sigma_{1*}-F_1\sigma_\mathrm{s}/\Gamma_\mathrm{s})-F_2\sigma_\mathrm{s}/\Gamma_\mathrm{s}]/(\tau b_0\sigma_{0*})$, $\chi_0\equiv(\Lambda^1_0/\omega_0)^2[F_2/\Gamma_\mathrm{s}-(F_1/\Gamma_\mathrm{s})^2]/(\tau b_0\sigma_{0*})$ and $C_0\equiv(\Lambda^1_0/\omega_0)^2(\sigma_{0*}\sigma_{1*}-F_1\sigma_\mathrm{s}/\Gamma_\mathrm{s})^2/(\tau b_0\sigma_{0*})$ stand for nonlinear frequency shift, ion Compton scattering and shielded-ion scattering, respectively.

Equation (6) describes the test TAE Ω_0 evolution due to nonlinear interaction with the background TAE Ω_1. It is also the nonlinear parametric dispersion relation describing Ω_1 decaying into Ω_0 and Ω_s. Detailed analyses of equation (6) demonstrated that the scattering cross-section is significantly enhanced due to plasma nonuniformity [35]. In addition, the change of spontaneous decay condition indicated that TAE tends to decay into higher n sidebands [35], instead of lower ω sidebands in the uniform plasma limit [32]. While the present analysis accounts for only nonuniformity associated with density profile, inclusion of plasma temperature nonuniformity is expected to only quantitatively modify the scattering cross-section, leaving the qualitative picture that TAE spectral transfer in k_θ space in nonuniform plasmas unchanged. This motivates us to investigate the spectrum evolution of TAE in k_θ space in the next section, by extending equation (6) to include the interaction with multiple background TAEs.

3. Wave-kinetic equation for TAE spectrum evolution

In this section, the wave-kinetic equation describing the nonlinear evolution of the TAE spectral intensity is derived, and then transformed into k_θ space, in correspondence with TAEs' cascading behaviour in k_θ due to plasma nonuniformity [35].

As we mentioned before, only one background TAE is considered in equation (6). To take all the background TAEs into account, we summarise the nonlinear coupling term over k_1 and get

$$\varepsilon_{A0}|\delta\phi_0|^2 = -\sum_{k_1}\left(\Delta + \chi_0\varepsilon_{s*} - \frac{C_0}{\varepsilon_{s*}}\right)|\delta\phi_0|^2|\delta\phi_1|^2. \quad (7)$$

Equation (7) describes the evolution of test TAE Ω_0 due to interaction with all the background TAEs, with the lower-n background TAEs contributing to its nonlinear drive and higher-n TAEs contributing to nonlinear damping. Taking the imaginary part of equation (7), we obtain

$$\frac{\partial_t - 2\gamma_L}{\omega_{0R}}|\delta\phi_0|^2 = -\sum_{k_1}\left(\chi_0 + \frac{C_0}{|\varepsilon_{s*}|^2}\right)\varepsilon_{s*,I} \times |\delta\phi_0|^2|\delta\phi_1|^2. \quad (8)$$

In deriving equation (8), we have expanded $\varepsilon_{A0} \simeq \mathrm{i}(\gamma - \gamma_L)\partial_{\omega_{0R}}\varepsilon_{A0,R} \simeq 2\mathrm{i}(\gamma - \gamma_L)/\omega_{0R}$, with $\gamma \equiv \partial_t \ln\delta\phi_0$ and $\gamma_L \equiv \varepsilon_{A0,I}/\partial_{\omega_{0R}}\varepsilon_{A0,R}$ being the linear growth rate of $\boldsymbol{\Omega}_0$. Here, subscripts 'R' and 'I' stand for the real and imaginary parts respectively.

To proceed with equation (8) analytically, we consider a radial-mode-width-averaged spectral intensity for the potential fluctuation induced by TAE [40]. Specifically, we assume $|\delta\hat{\phi}_0|^2 \equiv (e/T_e)^2|\delta\phi_0|^2 = I_0\exp[-(x_0 - \Delta_0/2)^2/\Delta_0^2]$ for the test TAE and $|\delta\hat{\phi}_1|^2 \equiv (e/T_e)^2|\delta\phi_1|^2 = I_1\exp[-(x_1 + \Delta_1/2)^2/\Delta_1^2]$ for background TAEs propagating oppositely to the test TAE. Here, $x_k \equiv (nq - m)/(nq')$ with q being the safety factor, $I_k = I(k_\theta)$ is the spectral intensity, and $\Delta_k \equiv -1/(k_\theta S)$ is the distance between the neighbouring mode rational surfaces with S being the magnetic shear. Consequently, the wave-kinetic equation can be evaluated at the maxima of the test TAE fluctuation amplitude (i.e. $x_0 = \Delta_0/2$) where k_{r0} vanishes and an appropriate nonlocal expression for the perpendicular coupling term is $(\hat{\boldsymbol{b}}\cdot\boldsymbol{k_0}\times\boldsymbol{k_1})^2 = k_{\theta 0}^2|\partial/\partial x_1 \ln\delta\phi_1|^2$. Inevitably, this approximation brings overestimated nonlinear coupling coefficient due to the simplification of radial overlap effects.

To perform the mode summation, following [40], we adopt the continuum approximation. The summation over n_1 and m_1 can be expressed in the form of integration over $k_{\theta 1}$ and x_1,

$$\begin{aligned}\sum_{k_1} &= \sum_{n_1,m_1} = \int \mathrm{d}n_1\mathrm{d}m_1 = \int\left|\frac{\partial(n_1,m_1)}{\partial(k_{\phi 1},x_1)}\right|\mathrm{d}k_{\phi 1}\mathrm{d}x_1\\ &= \int|n_1 q' R|\mathrm{d}k_{\phi 1}\mathrm{d}x_1 = \int_0^\infty |k_{\phi 1}|R^2 q'\mathrm{d}k_{\phi 1}\int_{-\infty}^{\infty}\mathrm{d}x_1\\ &\simeq -\frac{rS}{q}\int_0^{-\infty}\mathrm{d}k_{\theta 1}|k_{\theta 1}|\int_{-\infty}^{\infty}\mathrm{d}x_1. \end{aligned} \quad (9)$$

Equation (8) can be further simplified for the subsequent analyses, i.e. keeping only the dominant ion Compton scattering term, and evaluating $\sigma_{0*} \simeq 1$ and $F_2 - F_1^2/\Gamma_s \simeq \rho_i^4(\boldsymbol{k}_{\perp 0}\cdot\boldsymbol{k}_{\perp 1})^2/4$ at $b \equiv k_\perp^2\rho_i^2/2 \lesssim 1$. In simplifying $\varepsilon_{s*,I}$, considering $\omega_s \ll \omega_{*i,s} \ll \omega_T$, we further expand $\omega_s = \omega_0 - \omega_1 \simeq (k_{\theta 1} - k_{\theta 0})\partial\omega/\partial k_{\theta 0}$, and evaluate $k_{\parallel s} = 1/(2qR) - x_1/(qR\Delta_1)$ at $x_1 = -\Delta_1/2$. Given all these approximations, equation (8) is reduced to

$$\begin{aligned}\frac{\partial_t - 2\gamma_L}{\omega_{0R}}I_0 = &\frac{\sqrt{\pi}}{32}\tau^2\rho_i^9\left(\frac{\Omega_{ci}}{\omega_0}\right)^2\frac{rSR}{L_N b_0}\int_0^{-\infty}\mathrm{d}k_{\theta 1}|k_{\theta 1}|\\ &\times\int_{-\infty}^{\infty}\mathrm{d}x_1 k_{\theta 0}^4 k_{\theta 1}^2\frac{(x_1+\Delta_1/2)^2}{\Delta_1^4}(k_{\theta 0}-k_{\theta 1})I_0 I_1\\ &\times\exp\left[-\left(\frac{qR}{v_i}\right)^2(k_{\theta 1}-k_{\theta 0})^2\left(\frac{\partial\omega}{\partial k_{\theta 0}}\right)^2\right]\\ &\times\exp\left[-\frac{(x_1+\Delta_1/2)^2}{\Delta_1^2}\right]. \end{aligned} \quad (10)$$

The integration over x_1 is straightforward, and equation (10) reduces to

$$\begin{aligned}\frac{\partial_t - 2\gamma_L}{\omega_{0R}}I_0 = &-\frac{\pi}{32}\tau^2\left(\frac{\Omega_{ci}}{\omega_0}\right)^2\rho_i^7\frac{rS^2R}{L_N}\int_0^{-\infty}\mathrm{d}k_{\theta 1}|k_{\theta 1}|k_{\theta 0}^2 k_{\theta 1}^3\\ &\times(k_{\theta 0}-k_{\theta 1})\exp\left[-\left(\frac{qR}{v_i}\right)^2(k_{\theta 1}-k_{\theta 0})^2\right.\\ &\left.\times\left(\frac{\partial\omega}{\partial k_{\theta 0}}\right)^2\right]I_0 I_1, \end{aligned} \quad (11)$$

which corresponds to summarizing background TAEs located at different radial positions with different poloidal mode numbers. Note that in equation (11), the exponential term indicates that only background TAEs with close poloidal wavenumber to the test TAE can contribute significantly to the nonlinear term. Without loss of generality, this 'close interaction' allows us to expand $I_1 = I(k_{\theta 1}) \simeq I(k_{\theta 0}) + (k_{\theta 1} - k_{\theta 0})\partial I/\partial k_{\theta 0}$ and integrate equation (11) over $k_{\theta 1}$. In the meantime, re-organizing the derived equation as a dimensionless form and replacing $k_{\theta 0}$ with its absolute value, we obtain

$$\begin{aligned}\frac{\partial_t - 2\gamma_{\mathrm{L}}}{\omega_{0\mathrm{R}}} I\left(\hat{k},t\right) AB^6\hat{k}^4 = &-\left[\frac{\sqrt{\pi}}{2}y\left(3+2y^2\right)\left(1+\mathrm{Erf}\left(y\right)\right)\right.\\ &\left.+e^{-y^2}\left(1+y^2\right)\right] I^2\left(\hat{k}\right)\\ &-\frac{1}{16B\hat{k}}\left[\sqrt{\pi}\left(15+4y^2\left(9+y^2\right)\right)\right.\\ &\left.\times\left(1+\mathrm{Erf}\left(y\right)\right)+2e^{-y^2}y\left(17+2y^2\right)\right]\\ &\times I\frac{\partial I}{\partial \hat{k}}. \end{aligned} \quad (12)$$

Here, $\hat{k} = |k_{\theta 0}\rho_{\mathrm{i}}|$, $A \equiv 32(\omega_0/\Omega_{\mathrm{ci}})^2 L_N\rho_{\mathrm{i}}/(\pi\tau^2 S^2 rR)$, $B \equiv (2qR/v_{\mathrm{i}})\partial\omega/\partial\hat{k}^2 \simeq (3/4+\tau)/(2\beta_{\mathrm{i}}^{1/2})$ with the linear dispersion relation $\omega = k_\parallel v_{\mathrm{A}}\sqrt{1+(3/4+\tau)k_\perp^2\rho_{\mathrm{i}}^2}$ containing the lowest order FLR effects used and β_{i} contributed by only thermal ions. $y \equiv B\hat{k}^2$, and $\mathrm{Erf}(y) \equiv 2/\sqrt{\pi}\int_0^y \exp(-\eta^2)\mathrm{d}\eta$ is the error function. Equation (12) is the desired form of wave-kinetic equation, with explicit dependence of the spectrum intensity I on $\hat{k}$ and t. Although it is difficult to solve analytically, we can numerically solve this time dependent partial differential equation as an initial value problem, which will be done in section 5.

Letting $\partial_t I(\hat{k},t) = 0$, equation (12) is reduced to an ordinary differential equation or the so-called fixed point form

$$\begin{aligned}\frac{2\gamma_{\mathrm{L}}}{\omega_{0\mathrm{R}}}AB^6\hat{k}^4 = &\left[\frac{\sqrt{\pi}}{2}y\left(3+2y^2\right)\left(1+\mathrm{Erf}\left(y\right)\right)\right.\\ &\left.+e^{-y^2}\left(1+y^2\right)\right] I\left(\hat{k}\right)\\ &+\frac{1}{16B\hat{k}}\left[\sqrt{\pi}\left(15+4y^2\left(9+y^2\right)\right)\right.\\ &\left.\times\left(1+\mathrm{Erf}\left(y\right)\right)+2e^{-y^2}y\left(17+2y^2\right)\right]\frac{\partial I}{\partial \hat{k}}. \end{aligned} \quad (13)$$

Equations (12) and (13) are the main results of the present work. It is worth noting that, both of them can be used to derive the TAE saturation spectrum with numerical solutions while the former can also describe the nonlinear temporal evolution of the TAE spectrum, as shown in section 5. On the other hand, the fixed point form is analytically tractable, which may provide us the approximate solutions of the saturation spectrum, as will be done in section 4.

Once the saturation spectrum is given, we can estimate the magnetic perturbation amplitude induced by TAE. Noting $|\delta B_r|^2 = |k_\theta \delta A_\parallel|^2$ and that $\delta\phi \sim \delta\psi$ for TAEs with predominantly ideal MHD condition, the saturation spectrum gives the overall perturbed magnetic field as

$$\begin{aligned}\left|\frac{\delta B_r}{B_0}\right|^2 &\sim \sum_k \frac{\tau^2}{4}\frac{\Omega_{\mathrm{ci}}^2}{\omega^2}\frac{e^2}{T_{\mathrm{e}}^2}k_\parallel^2 k_\theta^2\rho_{\mathrm{i}}^4|\delta\phi_k|^2\\ &= \frac{3\sqrt{\pi}}{16}\frac{\tau^2 r\rho_{\mathrm{i}}}{q^3R^2}\frac{\Omega_{\mathrm{ci}}^2}{\omega^2}\int \mathrm{d}\hat{k}\hat{k}^2 I_k. \end{aligned} \quad (14)$$

4. Fixed point analytic solution

The fixed point form equation (13) can be solved analytically at both long and short wavelength limits. For the long wavelength limit, we mean $y \equiv B\hat{k}^2 \ll 1$, i.e. $\hat{k}^2 \ll 2\beta_{\mathrm{i}}^{1/2}/(3/4+\tau)$. Keeping the lowest order of y in equation (13), the original equation is reduced to

$$\frac{\partial I}{\partial \hat{k}} + \frac{16}{15\sqrt{\pi}}B\hat{k}I = \frac{\gamma_{\mathrm{L}}}{\omega_{0\mathrm{R}}}\frac{32}{15\sqrt{\pi}}AB^7\hat{k}^5, \quad (15)$$

which can be solved as

$$I\left(\hat{k}\right) = e^{-P\hat{k}^2}\left(\int \frac{\gamma_{\mathrm{L}}}{\omega_{0\mathrm{R}}}\frac{32}{15\sqrt{\pi}}AB^7\hat{k}^5 e^{P\hat{k}^2}\mathrm{d}\hat{k} + C_1\right). \quad (16)$$

Here, $P \equiv 8B/(15\sqrt{\pi})$, C_1 is the integral constant to be determined. Noting that $\gamma_{\mathrm{L}} \equiv \gamma_{\mathrm{L}}(\hat{k})$, the approximate solution in the long wavelength limit can be obtained with an explicit expression of $\gamma_{\mathrm{L}}(\hat{k})$ provided. For instance, considering $\gamma_{\mathrm{L}}(\hat{k})$ as a constant, equation (16) gives us the scaling of $I(\hat{k}) \propto \hat{k}^6$ in long wavelength limit.

In the short wavelength limit, we have $y = B\hat{k}^2 \gg 1$, i.e. $\hat{k}^2 \gg 2\beta_{\mathrm{i}}^{1/2}/(3/4+\tau)$. Keeping the highest order of y in equation (12), the original equation is reduced to

$$\frac{\partial I}{\partial \hat{k}} + \frac{4}{\hat{k}}I = \frac{\gamma_{\mathrm{L}}}{\omega_{0\mathrm{R}}}\frac{4}{\sqrt{\pi}}AB^3\hat{k}^{-3}, \quad (17)$$

which can be solved as

$$I\left(\hat{k}\right) = \hat{k}^{-4}\left(\int \frac{\gamma_{\mathrm{L}}}{\omega_{0\mathrm{R}}}\frac{4}{\sqrt{\pi}}AB^3\hat{k}\mathrm{d}\hat{k} + C_2\right). \quad (18)$$

Here, C_2 is the integral constant to be determined. Similarly, in this short wavelength limit, the approximate solution can be derived with an explicit expression of $\gamma_{\mathrm{L}}(\hat{k})$. Considering $\gamma_{\mathrm{L}}(\hat{k})$ as constant, we have the scaling of $I(\hat{k}) \propto \hat{k}^{-2}$. The saturation spectrum of TAE can thus be obtained by fitting the long and short wavelength solutions using, e.g. Pade's approximation. This can be done straightforwardly as the $\gamma_{\mathrm{L}}(\hat{k})$ is given.

To check the validity of this analytical solution, a comparison between analytical and numerical solutions of equation (13) is given in figure 1, with the linear growth rate γ_{L} set as a constant and the numerical solution obtained by the fourth-order Runge–Kutta method. We note that, while we use constant γ_{L} as an example here for simplicity of analytical solution, the fixed point solution shall not exist, as TAEs are linearly unstable over the whole spectrum.

Note that in figure 1, the analytical solution shows good agreement with the numerical solution especially in short wavelength region. In the long wavelength region, the correspondence seems weaker due to the gradual invalidity of $\hat{k} \ll \sqrt{2\beta_{\mathrm{i}}^{1/2}/(3/4+\tau)} \simeq 0.3$. Generally, the analytic approximate solutions (16) and (18) are demonstrated to be valid. In this circumstance, once the linear growth rate distribution $\gamma_{\mathrm{L}}(\hat{k})$ or the corresponding approximate formulas in long and short wavelength limits are provided, the TAE saturation spectrum in long and short wavelength regions can be recovered.

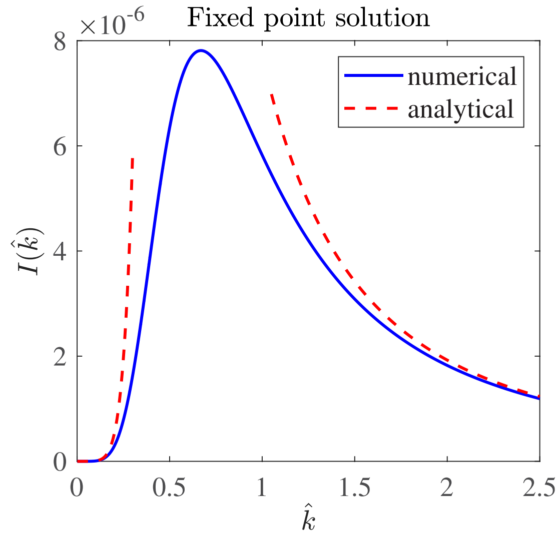

Figure 1. Fixed point solutions with constant $\gamma_L/\omega_{0R} \equiv 0.01$ in both analytical and numerical computation.

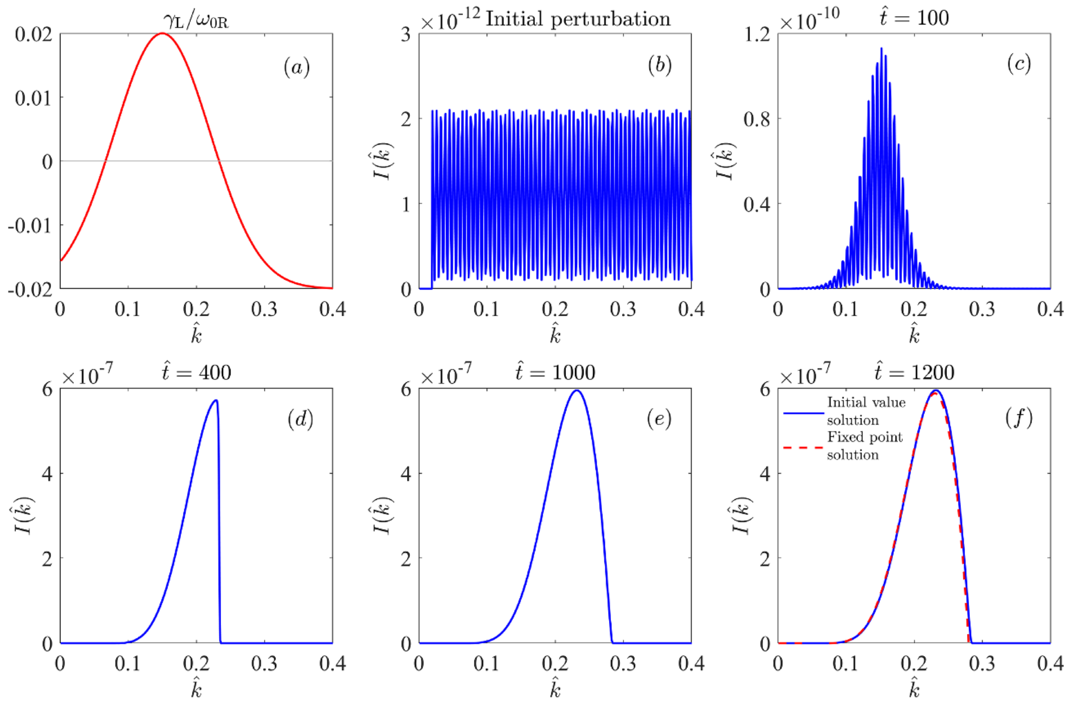

Figure 2. Plots of TAE spectrum evolution and saturation process by initial value solution and comparison with fixed point solution. Here, $\hat{t} \equiv \omega_{0R} t$, figures (*a*) and (*b*) are the provided linear growth rate distribution and random initial perturbation respectively. The evolution and saturation process of TAE spectrum is shown in figures (*c*)–(*e*). A comparison of the final saturation spectrum with fixed point solution is given in figure (*f*).

5. Application to reactor-relevant parameter region

In this section, the wave-kinetic equation (12) and the corresponding fixed point form equation (13) are applied to a reactor-relevant case, and the nonlinear evolution and saturation process of TAE spectrum are investigated by numerical solution.

Since the saturation spectrum depends sensitively on the distribution of $\gamma_L(\hat{k})$, a reactor-relevant case is adopted. Considering the radial location at $r/a \simeq 0.2$ with a being the minor radius, we take the TAE spectrum to be linearly unstable at the range of $n = 10 - 50$ and most unstable at $n = 30$ [5, 6]. Other parameters are taken as ITER relevant values like $B_0 = 5.3$ T, $R = 6.2$ m, $a = 2$ m, $\beta_i = 0.01$, $q = 1$, $S = 0.1$, and $R/L_N = 5$. The corresponding $\gamma_L(\hat{k})$ distribution is shown in figure 2(*a*). Given a random initial perturbation like figure 2(*b*), the nonlinear evolution process of TAE spectrum is obtained by numerically solving the wave-kinetic equation (12). In figure 2(*c*), the TAE spectrum intensity increases due to the linear drive of γ_L, and it is driven to a maximized intensity after hundreds of Alfvén times, as shown in figure 2(*d*). Note that with the most unstable mode shifted towards larger $|k_\theta|$, the nonlinear interaction term has already taken effects. However, due to the limitation of 'close interaction', the linear stable region ($\hat{k} \gtrsim 0.23$) stays unexcited. Later, the linear stable region is excited gradually due to the nonlinear drive by nearby unstable modes, and finally the TAE spectrum reaches a steady state, as shown in figures 2(*e*) and (*f*). The TAE saturation spectrum can also be obtained from the fixed point solution, i.e. the numerical solution of equation (13), as shown by the dashed curve in figure 2(*f*), in great agreement with initial value solution.

Recalling equation (14), with the TAE saturation spectrum computed above, we can estimate the resultant magnetic perturbation amplitude as $|\delta B_r/B_0| \sim \mathcal{O}(10^{-4})$. Compared with the previous results in uniform plasma regime [32], plasma nonuniformity provides a stronger suppression effect to the TAE spectrum due to the enhanced nonlinear coupling, as demonstrated in the previous work [35]. However, we need to emphasize again that the nonlinear coupling in this work is overestimated due to the simplified radial overlap effects, as discussed in section 3. This could lead to a smaller saturation amplitude, and the quantitative influence remains to be examined.

6. Conclusion and discussion

In this paper, based on the parametric dispersion relation obtained in the three wave parametric decay model, the wave-kinetic equation describing TAE spectrum evolution via ion induced scattering in nonuniform plasmas is derived and analysed. Generally speaking, with the explicit linear growth rate distribution $\gamma_{\rm L}(k_\theta)$ provided, the nonlinear evolution and saturation of TAE spectrum can be obtained by numerically solving the wave-kinetic equation. As anticipated, the entire TAE spectrum evolves towards larger $|k_\theta|$, and the linear stable region is excited nonlinearly by nearby unstable modes. On the other hand, the fixed point form of the wave-kinetic equation can be solved analytically. By expanding the nonlinear coupling coefficients at small or large $|k_\theta|$, the TAE saturation spectrum at both long wavelength ($k_\theta^2\rho_{\rm i}^2 \ll 2\beta_{\rm i}^{1/2}/(3/4+\tau)$) and short wavelength ($k_\theta^2\rho_{\rm i}^2 \gg 2\beta_{\rm i}^{1/2}/(3/4+\tau)$) can be obtained with the assumed $\gamma_{\rm L}(k_\theta)$ in both limits provided.

Compared with previous work on ion induced scattering in uniform plasmas [32], the TAE saturation amplitude derived here shows a significant reduction. Specifically, for typical reactor-relevant parameters, the magnetic perturbation amplitude induced by the TAE saturation spectrum is estimated as $|\delta B_r/B_0| \sim \mathcal{O}(10^{-4})$. This is expected due to the enhanced nonlinear coupling induced by plasma nonuniformity. However, we need to point out that the TAE saturation amplitude derived in the present work could be over-suppressed, due to the simplified radial overlap effects, while the quantitative influence remains to be examined.

On the other hand, with the TAE saturation spectrum derived in this work, it is feasible to estimate the influence on EP transport by quasi-linear transport theory. Meanwhile, considering that the TAE spectrum exhibits an evident energy transfer to larger k_θ modes, this evolution process driven by ion induced scattering in nonuniform plasmas could involve considerable momentum transport, which could contribute to the plasma intrinsic rotation, with potential beneficial effects to the plasma confinement. This is, however, beyond the scope of the present work and will be investigated in a future publication.

As a final remark, the saturation mechanism and spectrum evolution process presented in this work require verification by large-scale simulations. A simulation of three wave parametric decay process with the pump TAE driven by an antenna is in progress, which may provide a qualitatively picture of the mode coupling process. However, to study the nonlinear spectrum evolution in a reactor, a linear instability spectrum of TAEs is necessary to reflect the linear drive of EPs at different scales. Thus multiple modes simulation of TAEs driven by EPs is required, which may introduce other channels of nonlinearity, e.g. wave-particle nonlinearity, into the system and complicate the analysis.

Acknowledgments

This work was supported by National Key R&D Program of China under Grant No. 2024YFE03170000, the Strategic Priority Research Program of Chinese Academy of Sciences under Grant No. XDB0790201, the National Science Foundation of China under Grant Nos. 12275236 and 12261131622, and Italian Ministry for Foreign Affairs and International Cooperation Project under Grant No. CN23GR02.

ORCID iDs

Zhiwen Cheng 0009-0006-1426-0673
Kexun Shen 0000-0002-0512-6273
Fulvio Zonca 0000-0002-9270-4704
Zhiyong Qiu 0000-0002-7548-8819

References

[1] Tomabechi K., Gilleland J., Sokolov Y. and Toschi R. (ITER Team) 1991 *Nucl. Fusion* **31** 1135
[2] Alfvén H. 1942 *Nature* **150** 405–6
[3] Fasoli A. *et al* 2007 *Nucl. Fusion* **47** S264
[4] Chen L. and Zonca F. 2016 *Rev. Mod. Phys.* **88** 015008
[5] Wang T., Qiu Z., Zonca F., Briguglio S., Fogaccia G., Vlad G. and Wang X. 2018 *Phys. Plasmas* **25** 062509
[6] Ren Z., Chen Y., Fu G. and Wang Z. 2020 *Nucl. Fusion* **60** 016009
[7] Chen L. 1999 *J. Geophys. Res.: Space Phys.* **104** 2421
[8] Chen L. and Zonca F. 2007 *Nucl. Fusion* **47** 886
[9] Ishikawa M. *et al* (The JT-60 Team) 2005 *Nucl. Fusion* **45** 1474
[10] Zonca F., Chen L., Briguglio S., Fogaccia G., Milovanov A.V., Qiu Z., Vlad G. and Wang X. 2015 *Plasma Phys. Control. Fusion* **57** 014024
[11] ITER Physics Expert Group on Energetic Particles, Heating and Current Drive and ITER Physics Basis Editors 1999 *Nucl. Fusion* **39** 2471
[12] Ding R. *et al* 2015 *Nucl. Fusion* **55** 023013

[13] Chen L. and Hasegawa A. 1991 *J. Geophys. Res.: Space Phys.* **96** 1503
[14] Falessi M.V. and Zonca F. 2019 *Phys. Plasmas* **26** 022305
[15] Chen L. 1994 *Phys. Plasmas* **1** 1519
[16] Cheng C., Chen L. and Chance M. 1985 *Ann. Phys., NY* **161** 21
[17] Chen L. 1988 On resonant excitation of high-n magnetohydrodynamic modes by energetic/alpha particles in tokamaks *Theory of Fusion Plasmas* ed SIF (Association EUROATOM, Bologna) p 327
[18] Wong K.L. *et al* 1991 *Phys. Rev. Lett.* **66** 1874–7
[19] Heidbrink W.W. 2008 *Phys. Plasmas* **15** 055501
[20] Spong D.A., Bass E.M., Deng W., Heidbrink W.W., Lin Z., Tobias B., Van Zeeland M.A., Austin M.E., Domier C.W. and Luhmann N.C.J. 2012 *Phys. Plasmas* **19** 082511
[21] Zonca F. and Chen L. 2014 *Phys. Plasmas* **21** 072120
[22] Hahm T.S. and Chen L. 1995 *Phys. Rev. Lett.* **74** 266
[23] Chen L. and Zonca F. 2012 *Phys. Rev. Lett.* **109** 145002
[24] Chen L. and Zonca F. 2013 *Phys. Plasmas* **20** 055402
[25] Qiu Z., Chen L. and Zonca F. 2023 *Rev. Mod. Plasma Phys.* **7** 28
[26] Zonca F., Romanelli F., Vlad G. and Kar C. 1995 *Phys. Rev. Lett.* **74** 698
[27] Todo Y., Berk H.L. and Breizman B.N. 2012 *Nucl. Fusion* **52** 094018
[28] Qiu Z., Chen L. and Zonca F. 2016 *Phys. Plasmas* **23** 090702
[29] Qiu Z., Chen L. and Zonca F. 2017 *Nucl. Fusion* **57** 056017
[30] Chen L., Qiu Z. and Zonca F. 2022 *Nucl. Fusion* **62** 094001
[31] Liu P., Wei X., Lin Z., Brochard G., Choi G.J., Heidbrink W.W., Nicolau J.H. and McKee G.R. 2022 *Phys. Rev. Lett.* **128** 185001
[32] Qiu Z., Chen L. and Zonca F. 2019 *Nucl. Fusion* **59** 066024
[33] Chen L. and Zonca F. 2011 *Europhys. Lett.* **96** 35001
[34] Chen L., Qiu Z. and Zonca F. 2022 *Phys. Plasmas* **29** 050701
[35] Cheng Z., Shen K. and Qiu Z. 2024 *Nucl. Fusion* **64** 066031
[36] Connor J.W., Cowley S.C., Hastie R.J. and Pan L.R. 1987 *Plasma Phys. Control. Fusion* **29** 919
[37] Diamond P.H., McDevitt C.J., Gürcan O.D., Hahm T.S. and Naulin V. 2008 *Phys. Plasmas* **15** 012303
[38] Diamond P.H., McDevitt C.J., Gürcan O.D., Hahm T.S., Wang W.X., Yoon E.S., Holod I., Lin Z., Naulin V. and Singh R. 2009 *Nucl. Fusion* **49** 045002
[39] Frieman E.A. and Chen L. 1982 *Phys. Fluids* **25** 502–8
[40] Hahm T.S. and Tang W.M. 1991 *Phys. Fluids B* **3** 989–99